COBEM 2021 26th International Congress of Mechanical Engineering
November 22-26, 2021, Virtual Congress, Brazil

COB-2021-0962 CLADDED PIPES RESIDUAL STRESS ANALYSIS

Gustavo Borcard da Silva
Pedro Palmeirim Athayde Martins
Rodrigo Braga da Silva
Departamento de Engenharia Mecânica - PPEMM - CEFET/RJ; Av. Maracanã, 229 – RJ – Brazil.
gustavo.borcard@aluno.cefet-rj.br, pedro.athayde@ aluno.cefet-rj.br, rodrigo.braga@ aluno.cefet-rj.br

Letícia Campos
Programa de Pós-graduação em Engenharia Mecânica e Tecnologia de Materiais - PPEMM - CEFET/RJ; Av. Maracanã, 229 – RJ – Brazil.
leticia.campos@ aluno.cefet-rj.br

Paulo Pedro Kenedi
Programa de Pós-graduação em Engenharia Mecânica e Tecnologia de Materiais - PPEMM - CEFET/RJ; Av. Maracanã, 229 – RJ – Brazil. Departamento de Engenharia Mecânica – CEFET/RJ - Av. Maracanã, 229 – RJ – Brazil.
paulo.kenedi@cefet-rj.br

Abstract. *The Brazilian Pre-Salt reservoirs are located in ultra-deep depth and contain a quite corrosive petroleum. To exploit it, severe requirements against corrosion must be implemented to protect the production structures. For instance, cladding the internal riser surface with a corrosion resistant material, as Inconel 625, is widely used in the offshore industry. Although it is a corrosion resistance layer, it also plays a part in the load share, of the imposed bending moments, with the steel pipe. The cladded riser is reeled to be transported, inducing a considerable yielding of the rigid cladded riser cross sections. As the ship arrives to the launch point, the rigid riser is unreeled, allowing the spring back of this component. As a result, residual stress distributions, for both, steel pipe and cladded layer, arise. The proposed analytical model analyses the sharing load between both components, steel pipe and cladded layer, during the reeling and unreeling of a rigid cladded riser and the consequent cross section residual stress distribution formation. A comparative analysis, for specific geometry of commercial cladded risers, between the residual stresses on the outer diameter and on the elastoplastic border was implemented.*

Keywords: *Cladded pipes, residual stress, analytical model.*

1. INTRODUCTION

Due to increasing depths in offshore Brazilian oil exploration, the use of rigid risers has become more frequently. The need for innovation led to new technologies, including in the rigid risers field. In fact, the production of materials for rigid pipelines became more efficient and cheaper. The API 5L steels, used nowadays, has better weldability than steels produced in previous generations, as well as superior mechanical properties. To protect the rigid risers from the quite corrosive petroleum, of Pre-Salt, cladding the internal steel pipe surfaces has been used. It consists of the superficial deposition of a thin layer, that generated protection against corrosion, for instance, using Inconel ® 625 alloy.

The cladded rigid riser, named as cladded riser for now on, is produced on the coast and wounding onto the vessel reel, so that it can be transported to the desired location, with a subsequent unreeling. To do this the cladded riser cross sections must be partially yielded. As the cladded riser unreels as show in Fig. 1, the spring-back phenomenon occurs, and the residual stress distribution are produced.

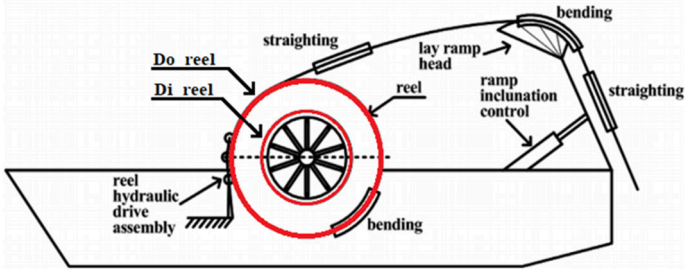

Figure 1 . Transport reel in vessel. Adapted by Cho *et al*. (2017).

Most articles of residual stresses are about the experimental approach, as described in Schajer (2013). The stress analysis of cladded structures is a topic that is quite uncommon in technical literature. There are few articles/papers about it submitted to bending moments, as in Silva (2018) and in Rody *et al*. (2014). The cold bending of metallic structures, resulting in partially yielded cross-sections, are more common, as in Fukuda *et al*. (2014), Rimovskis *et al*. (2012), Sen *et al*. (2011) and Riagusoff *et al*. (2010). The residual stresses cross section distribution, of partially yielded offshore structures, are also quite present in technical literature, as in de Castro *et al*. (2019), Zaidan and Kenedi (2019), Wang *et al*. (2018) and and Lopes (2013). In this work an analytic model, based in Mechanics of Solids, is proposed to estimate the residual stress cross section distribution, of a cladded riser, after a reel/unreel operation, present in its transportation process up to the launch site. The calculus was performed with the aid of a mathematical software, as Mathcad.

2. ANALYTICAL MODEL

In this section it will be presented all the steps necessary to develop an analytical model to estimate the sharing load between the steel pipe and the clad layer; when submitting the cladded riser to a bending moment, during the reeling process. After the unreeling process, with the spring-back generation, the cross-section residual stress distribution will be estimated for both, steel pipe and clad layer.

Constitutive Model

The bi-linear behavior of the materials can be modeled using, for instance, the modulus tangent E_t approach, Simo and Huges (2000). Equation (1) describes the relation between stress and strain for this application:

$$\sigma(\rho) = \begin{cases} E\,\dfrac{y}{\rho}\,, & \rho > \rho_y \;\; (elastic\ region) \\ S_y + E_t \cdot \left(\dfrac{y}{\rho} - \varepsilon_y\right), & \rho \le \rho_y \;\; (plastic\ region) \end{cases} \tag{1}$$

Where, $\sigma(\rho)$ is normal stress in function of the imposed curvature radius ρ, S_y is the yielding strength, E is the Young's modulus and y is the perpendicular distance between the neutral line to any cross-section point. The curvature radius that the structure begins to yield is estimated as:

$$\rho_y = \frac{E \cdot I}{M_y} \qquad \text{where} \qquad I = \frac{\pi\,(R_o^4 - R_i^4)}{4} \tag{2}$$

where I is the area moment of inertia of area, R_i is the internal radius and R_o is the external radius, M_y is the bending moment that begins to yield the structure (see equation (6)).

Geometry

Fig. 2.a shows an example of the geometry of the cladded riser cross-section. Figures 2.b. and 2.c show the two types of differential areas used in the analytical model.

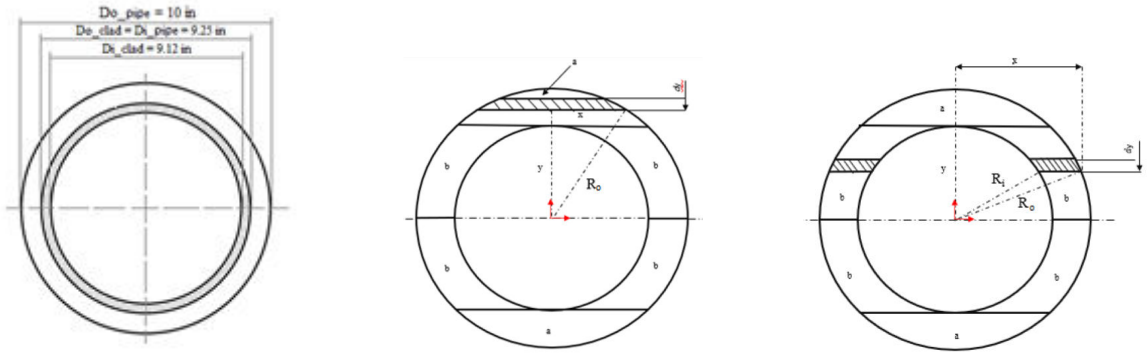

(a) (b) (c)

Figure 2. (a) an cross-section set example. The differential areas: (b) in "a" region with dA_a, (c) in "b" region with dA_b.

The differential areas are estimated as:

$$dA_a = 2 \cdot \sqrt{R_o^2 - y^2}\; dy \qquad dA_b = 2 \cdot \left[\sqrt{R_o^2 - y^2} - \sqrt{R_i^2 - y^2}\right] dy \tag{3}$$

The elastoplastic border y_y is the half height of the elastic core. The y_y lower limit is reached when M = M_y, so y_y = R_o and the upper limit is reached when M = M_p, so $y_y \approx 0$. For intermediary bending moments M(ρ), it is used:

$$y_y(\rho) = \varepsilon_y.\rho \quad for\ M_y \leq M(\rho) < M_p \tag{4}$$

Where M_y and M_p are estimated by, respectively, by equations (6) and (7). Fig. 3 show a three y_y phases. Fig. 3.a show when M(ρ) = M_y, the elastoplastic border is y_y = R_o. Both, Figures, 3.b and Fig. 3.c, are in $M_y \leq M(\rho) < M_p$ range, with the difference that Fig. 3.b is not so loaded as Fig. 3.c. Note the light gray represents the elastic core.

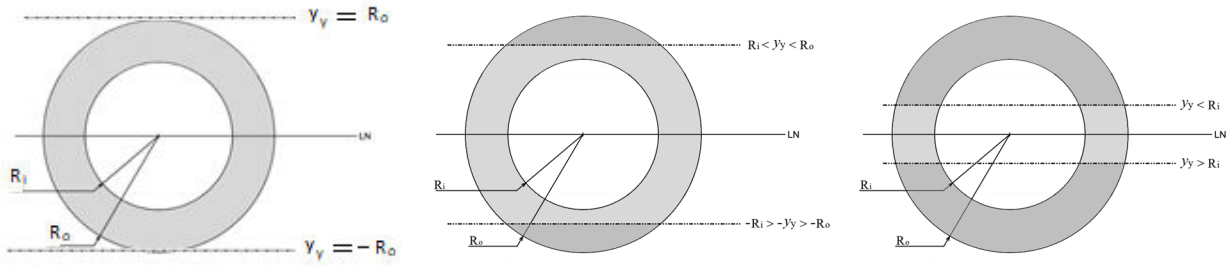

(a) (b) (c)

Figure 3. Elastoplastic border y_y for (a) $M(\rho) = M_y$, (b) $M_y \leq M_{\_a}(\rho) < M_p$, (c) $M_y \leq M_{\_b}(\rho) < M_p$.

Where $M_{\_a}(\rho)$ and $M_{\_b}(\rho)$ are bending moments in the range $M_y \leq M(\rho) < M_p$. $M_{\_a}(\rho)$ is the bending moment, shown in equation (8), with the elastoplastic border y_y is in region *a* (see Fig. 2.b) and $M_{\_b}(\rho)$ is the bending moment, shown in equation (9), with the elastoplastic border y_y is in region *b* (see Fig. 2.c).

Loading, spring-back and limit states

Equation (5) is used in the elastic range:

$$M_e(\rho) = \frac{E \cdot I}{\rho} \tag{5}$$

Equations (6) and (7) represent the two limit states of a pipe of internal radius R_i and the external radius R_o, submitted to a bending moment:

$$M_y = 2 \cdot \left[\int_0^{R_i} y \cdot \left(\frac{y}{R_o} \cdot S_y \right) \cdot 2 \cdot \left(\sqrt{|{R_o}^2 - y^2|} - \sqrt{|{R_i}^2 - y^2|} \right) dy + \int_{R_i}^{R_o} y \cdot \left(\frac{y}{R_o} \cdot S_y \right) \cdot 2 \cdot \left(\sqrt{|{R_o}^2 - y^2|} \right) dy \right] \tag{6}$$

$$M_p = 2 \cdot \left[\int_0^{R_i} y \cdot \left(S_y + E_t \cdot \left(\frac{y}{\rho} - \varepsilon_y \right) \right) \cdot 2 \cdot \left(\sqrt{|{R_o}^2 - y^2|} - \sqrt{|{R_i}^2 - y^2|} \right) dy + \int_{R_i}^{R_o} y \cdot \left(S_y + E_t \cdot \left(\frac{y}{\rho} - \varepsilon_y \right) \right) \cdot 2 \cdot \left(\sqrt{|{R_o}^2 - y^2|} \right) dy \right] \tag{7}$$

Between these limit states, for $M_y \leq M(\rho) < M_p$, there are two developed set of equations, depending on the location of the elastoplastic border, equation (8) as Fig. 3.b and equation (9) as Fig. 3.c:

$$\begin{aligned}
M_{y_a}(\rho) &= 2 \cdot \left[\int_0^{R_i} y \cdot \left(\frac{y}{\rho \cdot \varepsilon_y} \cdot S_y \right) \cdot 2 \cdot \left(\sqrt{|{R_o}^2 - y^2|} - \sqrt{|{R_i}^2 - y^2|} \right) dy + \int_{R_i}^{\rho \cdot \varepsilon_y} y \cdot \left(\frac{y}{\rho \cdot \varepsilon_y} \cdot S_y \right) \cdot 2 \cdot \left(\sqrt{|{R_o}^2 - y^2|} \right) dy \right] \\
M_{p_a}(\rho) &= 2 \cdot \left[\int_{\rho \cdot \varepsilon_y}^{R_o} y \cdot \left[S_y + E_t \cdot \left(\frac{y}{\rho} - \varepsilon_y \right) \right] \cdot 2 \cdot \left[\sqrt{|{R_o}^2 - y^2|} \right] dy \right] \\
M_{_a}(\rho) &= M_{y_a}(\rho) + M_{p_a}(\rho) \qquad \text{for } \rho_p < \rho < \rho_y
\end{aligned} \tag{8}$$

$$\begin{aligned}
M_{y_b}(\rho) &= 2 \cdot \left[\int_0^{\rho \cdot \varepsilon_y} y \left(\frac{y}{\rho \cdot \varepsilon_y} \cdot S_y \right) \cdot 2 \cdot \left(\sqrt{|{R_o}^2 - y^2|} - \sqrt{|{R_i}^2 - y^2|} \right) dy \right] \\
M_{p_b}(\rho) &= 2 \cdot \left[\int_{\rho \cdot \varepsilon_y}^{R_i} y \left(S_y + E_t \cdot \left(\frac{y}{\rho} - \varepsilon_y \right) \right) \cdot 2 \cdot \left(\sqrt{|{R_o}^2 - y^2|} - \sqrt{|{R_i}^2 - y^2|} \right) dy + \int_{R_i}^{R_o} y \left[S_y + E_t \left(\frac{y}{\rho} - \varepsilon_y \right) \right] \cdot 2 \cdot \left[\sqrt{|{R_o}^2 - y^2|} \right] dy \right] \\
M_{_b}(\rho) &= M_{y_b}(\rho) + M_{p_b}(\rho) \qquad \text{for } \rho_p < \rho < \rho_y
\end{aligned} \tag{9}$$

Note that all equations (5-9) can be used for both: steel pipe and clad layer. Fig. 4 is a graphical representation of equations (5), (8) and (9). In fact, Fig. 4 show the relation between the bending moment *M* and the radius of curvature ρ for: $M_e(\rho)$ (green curve), $M_{y\_a}(\rho)$ (blue curve) and $M_{\_b}(\rho)$ (red curve).

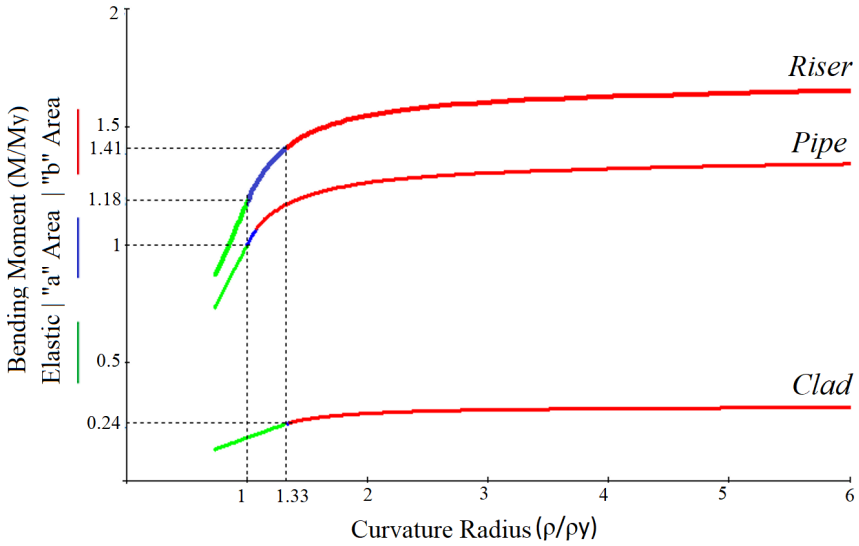

Figure 4. Bending Moment vs curvature radius. Graphical representation of equations: (5) with green curves, (8) with blue curves and (9) with red curves.

Note that as the steel pipe and the clad layer has different thicknesses, the extension, for instance, of blue lines of region *a* are, therefore, different.

Residual Stress

The residual stress distribution is formed through the addition of the load stress distribution, represented by equation (10), with the spring-back stress distribution, represented by equation (11), as in Castro and Meggiolaro (2016):

$$\sigma(\rho,y)=\begin{cases} const\cdot\left(S_y+E_t\cdot\left(\frac{y}{\rho}-\varepsilon_y\right)\right), & for\ y_y<y\le c \\ const\cdot\left(\frac{y}{\rho\cdot\varepsilon_y}\cdot S_y\right), & for-y_y<y\le y_y \\ const\cdot\left(-S_y+E_t\cdot\left(\frac{y}{\rho}-\varepsilon_y\right)\right), & for-c<y\le -y_y \end{cases} \tag{10}$$

Note that the const = -1 for positive M(ρ) and const = 1 for negative M(ρ). Once the bending moment is removed from the component, the spring-back will show up. Its stress distribution is described, as Crandall *et al*. (1978):

$$\sigma_{sb}(\rho,y)=\frac{-M(\rho)\,y}{I} \tag{11}$$

M (ρ) can be $M_{\_a}(\rho)$ or $M_{\_b}(\rho)$. Although the equation (11) produces $\sigma_{sb}(\rho,y)>S_y$, after the loading phase the material has at least $2\cdot S_y$ range to get through. So, the spring-back happens in a completely elastic way. The residual stress distribution is estimated by:

$$\sigma_R(\rho,y)=\sigma(\rho,y)+\sigma_{sb}(\rho,y) \tag{12}$$

The equation (12) is valid for a load and unload cycle. For more than one cycle, other concepts must be implemented to describe correctly the final residual stress distribution.

3. RESULTS

In this item the theory presented previously will be implemented with an example. Fig. 2.a show the geometry of the cladded riser used in this example. An API 5L X52 steel was selected for the material for the steel pipe and the Inconel ® 625 was selected for the clad layer. The Table 1 presents the mechanical properties of the used materials in this example.

Table 1. Mechanical properties of API 5L X52 and Inconel 625.

Properties	API 5L X52 (Pipe)	Inconel ® 625 (Clad layer)	unit
Young's Modulus (E)	207	207	GPa
Tangent Modulus (E_t)	1.24	0.82	GPa
Poisson's ratio (v)	0.3	0.297	-
Moment of Inertia of area (I)	$5.47 \cdot 10^{-5}$	$9.92 \cdot 10^{-6}$	m^4
Specific gravity (μ)	7860	8440	kg/m^3
Yield Stress (S_y)	360	442	MPa
Ultimate Stress (S_{ut})	460	896	MPa
Yield Strain (ε_y)	$1.74 \cdot 10^{-3}$	$2.13 \cdot 10^{-3}$	-
Ultimate Strain (ε_{ut})	0.08	0.55	-

3.1 Bending Moment distributions

Fig. 5 show an interesting graphic of the variation of the sharing loading between the steel pipe and the clad layer in function of the applied curvature radius.

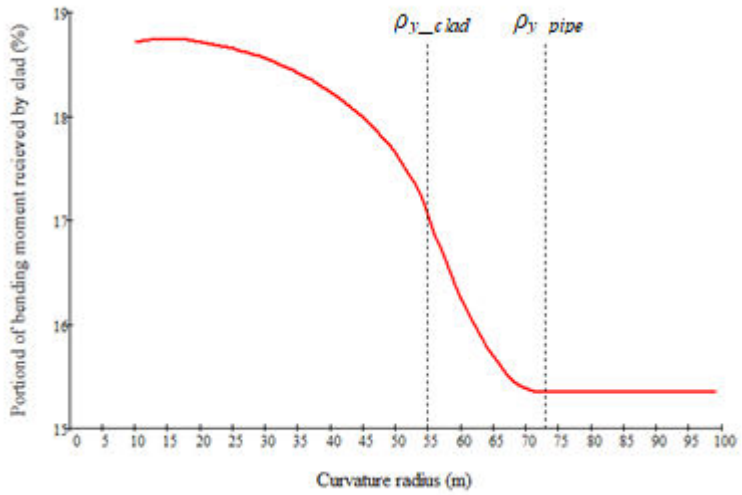

Figure 5. Share load - Percentual of clad layer contribution in function of the curvature radius.

The Fig. 5 shows that during the elastic part of the loading, the sharing loading maintains a constant value. But, as soon the loading begins to yield the cladded riser, a not intuitive phenomenon starts to occur: The increasing of clad layer participation in the load share as the curvature radius diminishes.

3.2 Stress distributions

The stresses generated by the loading and unloading process are directly related to the imposed curvature on the riser. In Fig. 6 shows, for this example of cladded riser, which cross- section geometry is disponible in Fig. 2.a and the mechanical properties are disponible in Table 1. Note that the cross section cladded riser are shown in Fig. 6 are not in the correct plane. They were represented in this way only to geometrically correlate the stress distribution curves with the position of the steel pipe and clad layer radius. The blue curves are related with the clad layer and the red curves are related to the steel pipe. The equations (10-12) were used for the load, spring-back and residual stress distribution, for both: steel pipe and clad layer.

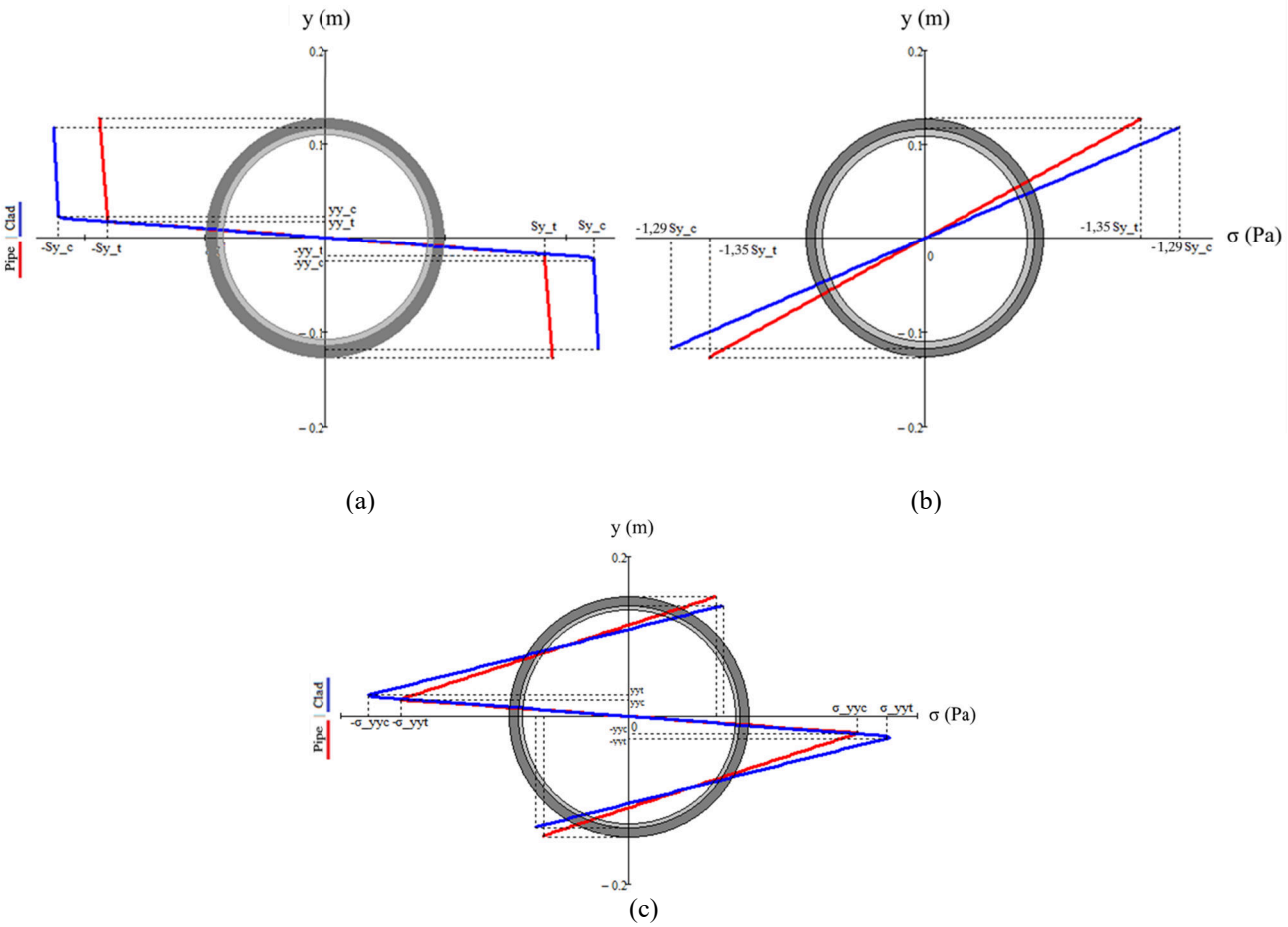

Figure 6. Cross-section stress distribution for both, steel pipe and clad layer: (a) Loading, (b)Unloading (spring-back) and (c) Residual.

The cross-section residual stress distributions, for both, steel pipe and clad layer, are shown in Fig.6. Note that, for this example, the maximum value is located in the clad layer elastoplastic border, not in the steel pipe.

Fig. 7 explicit an important part of the paper conclusions. For, this example, the curvature radius of the analytical model was varied from required to the steel pipe cross-section begins to yield, up to curvature radius that almost entirely yield the cross-section. The two curves, named y_y and R_o shows the parameterized residual stress $(\sigma_R(\rho, y)/\, S_y)$, respectively, at the elastoplastic border and at the steel pipe external radius.

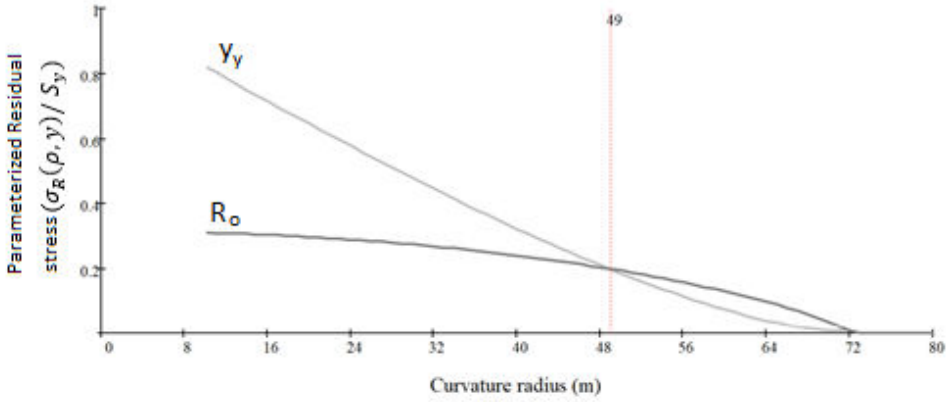

Figure 7. Position of the maximum residual stress - Turning point (Fish like Graphic).

Note that, for this example, only for relatively large curvature radius the parameterized residual stress is maximum at R_o. But for smaller curvature radius, which, in turn, is usual for offshore transportation reels, the parameterized residual stress is maximum at y_y.

3.3 Comparative results

Fig. 8, shows the range of commercial pipes and most common reels diameters. Each color represents the percentual difference of the residual stress values between y_y and in R_o. The colors changes from green to red, where green indicates when the percentual difference of the residual stress values between y_y and R_o is small, and red when the difference is as large as 200%.

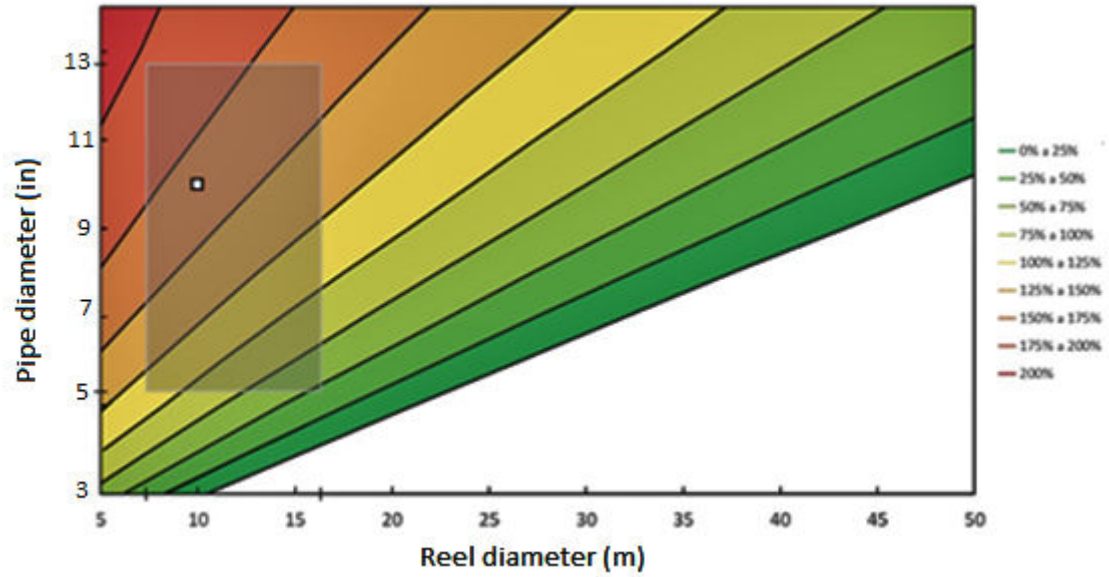

Figure 8. Graphical study of percentual difference of the residual stress values, positioned in y_y and in R_o.

The geometry defined in this paper is designated by the white dot in Fig.8. It represents that the residual stress at y_y is in a range from 150% up to 175% of to the residual stress verified at R_o. In fact, the residual stress at y_y is 164% larger than the stress at R_o, which is a quite significant difference. Note that if the experimental residual stress could only access the R_o position, the residual stresses results would be quite underestimated.

4. CONCLUSION

The proposed analytical model estimated the bending moment share load between the steel pipe and the clad layer of a cladded riser. After a reeling sequence, that consisted in reel and, in sequence, unreel the cladded riser, the residual stress distribution was estimated for both: steel pipe and clad layer. It was possible to verify that a layer of protection against corrosion, plays a role in structural resistance, besides the obviously corrosion protection. It receives up to 18% of the total moment imposed to the cladded riser set.

Although it is somehow expected that the maximum residual stresses of a cladded riser could occur at the external radius, for the curvature radius normally used to transport risers to the installation site the maximum residual stresses actually would occur at the elastoplastic border.

5. REFERENCES

API Specification 5L, 46th Edition.

Castro, J.T.P and Meggiolaro, M.A., 2016. *Fatigue design techniques, volume 2: low-cycle and multiaxial fatigue*. 1º. ed. Scotts Valley: CreateSpace.

Cho, J. R., Joo, B., Cho, J., Moon, Y. H., 2017. "Finite element analysis of the offshore reel-laying operations for double-walled pipe". *Advances in Mechanical Engineering*, Vol. 9, No. 10. https://doi.org/10.1177/1687814017731226.

Crandall, S.H., Dahl, N.C. and Lardner, T.J. 1978. *An introduction to the mechanics of solids. Second Edition with SI units*, New York. McGraw Hill International Editions.

De Castro, F.A., Kenedi, P.P., Vignoli, L.L., Riagusoff, I.I.T., 2019. "Residual stress distribution in hyperstatic beams". In *Proceedings of the 7th International Symposium on Solid Mechanics-MECSOL 2019*. São Carlos, São Paulo, Brazil.

Fukuda, N., Yatabe, H., Kawaguchi, S., *et al*., 2003. "Experimental and analytical study of cold bending process for pipelines". *J Offshore Mech Arctic Eng.* Vol.125, pp.153–157.

Lopes, D.G. 2013. *Avaliação das tensões residuais na montagem de conectores em armaduras de tração de dutos flexíveis*. M.Sc. dissertation (in portuguese). Centro Federal de Educação Tecnológica Celso Suckow da Fonseca—CEFET/RJ, Rio de Janeiro, Brazil, 2013.

Riagusoff, I.I.T., Kenedi, P.P., Souza, L.F.G., Pacheco, P.M.C.L., 2010. "Modeling of Pipe Cold Bending: A Finite Element Approach". In *Proceedings of the 6th Congresso Nacional de Engenharia Mecânica - CONEM 2010*, Campina Grande, Paraíba, Brazil.

Rimovskis, S. and Sabaliauskas, A., 2012. "Analysis of rectangular and circular cross-section power hardening elements under pure bending". *Int J Mater Eng*. Vol. 2, pp. 84–89.

Rody, P. H. C., Kenedi, P.P., Pacheco, P.M.C.L., 2014. "Cladded Pipes Stress Analysis". In *Proceedings of the 25º Congresso Nacional de Transporte Aquaviário - SOBENA 2014*, Rio de Janeiro. Brazil.

Schajer, G.S., 2013. *Practical residual stress measurements methods*. Hoboken: Wiley.

Sen, M., Cheng, J.J.R. and Zhou, J., 2011. "Behavior of cold bend pipes under bending loads". *J Struct Eng*. Vol. 137, No. 5, pp. 571–578.

Simo, J. C. and Hughes, T. J. R., 2000. *Computational Inelasticity*. Springer.

Silva, R. D., 2018. *Estudo de liga de níquel alternativa na união de tubos de aço API 5L X65 revestidos internamente com Inconel 625* (in Portuguese). Master Thesis, Universidade Federal do Ceará, Fortaleza, Brazil.

Wang, J. and Mirzaee-Sisan, A., 2018. "The effect of plasticity on residual stress generation and redistribution in offshore pipelines". *Int J Press Vessels Pip*. Vol.159, pp.101–110.

Zaidan, D.L., Kenedi, P.P., 2019. "Influence of Residual Stresses in Fatigue Life of Partially Yielded Mechanical Parts". In *Proceedings of the 5th ABCM International Congress of Mechanical Engineering - COBEM 2019*, Uberlândia, Minas Gerais. Brazil.

6. RESPONSIBILITY NOTICE

The authors are the only responsible for the printed material included in this paper.